

Improving Strength of Postbuckled Panels Through Stitching

Dawn C. Jegley

Mail Stop 190

NASA Langley Research Center Hampton, VA 23681

Abstract

The behavior of blade-stiffened graphite-epoxy panels with impact damage is examined to determine the effect of adding through-the-thickness stitches in the stiffener flange-to-skin interface. The influence of stitches is evaluated by examining buckling and failure for panels with failure loads up to 3.5 times greater than buckling loads. Analytical and experimental results from four configurations of panel specimens are presented. For each configuration, two panels were manufactured with skin and flanges held together with through-the-thickness stitches introduced prior to resin infusion and curing and one panel was manufactured with no stitches holding the flange to the skin. No mechanical fasteners were used for the assembly of any of these panels. Panels with and without low-speed impact damage were loaded to failure in compression. Buckling and failure modes are discussed. Stitching had little effect on buckling loads but increased the failure loads of impact-damaged panels by up to 30%.

Key Words: Graphite-epoxy, Aircraft, Composite, Stitching, Buckling, Postbuckling, Debond

1. Introduction

In a broad sense, goals of the NASA aeronautics program include reducing the cost of air travel, reducing the emissions from aircraft and developing enabling technology to make possible revolutionary air vehicles. To achieve these goals, NASA has been involved in the

development of technologies needed for future low-cost, light-weight composite structures for commercial transport aircraft with potential applications to more futuristic vehicles. Lighter aircraft burn less fuel and, therefore, cost less to operate and produce less noise and fewer emissions. As a consequence of the effort to build lighter aircraft, a stitched graphite-epoxy material system has been developed with the potential for reducing the weight, manufacturing cost and operational cost of commercial transport aircraft wing structure [1,2]. By stitching through the thickness of a dry pre-stacked skin and then stitching together the stringers, intercostals and spar caps with the skin, the need for mechanical fasteners in a wing box is almost eliminated.

Revolutionary changes in the material system and manufacturing method are not the only ways to reduce structural weight. One method of reducing aircraft weight is to allow structural components such as wing skins to buckle at loads less than Design Ultimate Load (DUL). Allowing buckling at loading less than design ultimate load, and even less than design limit load requires that the structure have significant postbuckling strength, that its behavior be predictable and consistent, and that the interaction of the buckling deformations with manufacturing or service anomalies such as impact damage or minor geometric imperfections be understood and considered in the design process.

One of the most critical problems leading to failure in stiffened composite structure is the tendency for the stiffener flange to separate or debond from the skin. This skin-flange separation has been identified as the primary failure mechanism for panels subjected to compression, pressure and/or shear loadings and in panels demonstrating postbuckling behavior [3-8]. The influence of stitching on the separation of the flange from the stringer, examined in references 9 and 10, indicate that stitching can significantly improve the debonding resistance of graphite-

epoxy panels. The objective of this study is to determine the effectiveness of stitches in preventing debonding in undamaged and impact-damaged buckled graphite-epoxy panels. A series of specimens were designed to evaluate the influence of impact damage on postbuckled behavior of thin-skinned compression-loaded panels. Analytical and experimental results from these panels are presented herein. Since impact damage has been a critical factor in the design of composite aircraft structure [3,11,12], the problem of skin-stiffener separation is examined in both undamaged and impact-damaged panels.

2. Test specimen description

Four panel configurations representative of an upper wing skin were examined in this study. Each configuration contains a skin and four blade-stiffeners. A sketch of a panel is shown in figure 1 and the measured geometry is described in table 1 for the control specimens. Since panel geometry (thicknesses, heights) was found to be consistent within each panel configuration, only detailed measurements from control panels are presented. Nominal skin thicknesses range from 2.8 mm to 5.6 mm (0.11 to 0.22 in.). Blade thicknesses are either 11.2 or 14.0 mm (0.44 or 0.55 in.). Stiffener spacing is 203 mm (8.0 in.). All panels contain a test section 686 mm (27 in.) long. Panel widths are approximately 687 mm (26.65 in.). All blade heights are either 64.5 or 82.3 mm (2.54 or 3.24 in.), as shown in table 1. Three panels of each of the four configurations were loaded in compression to failure. The composite skin and blade-stiffeners were composed of layers of graphite material forms that were pre-kitted in nine-ply stacks using Hercules, Inc. AS4 fibers. Each nine-ply stack had a $[45/-45/0_2/90/0_2/-45/45]_T$ laminate stacking sequence and was approximately 1.4 mm (0.055 in.) thick. Several stacks of

the pre-kitted material were used to build up the desired thickness at each location. All material was stitched together using E. I. DuPont de Nemours, Inc. Kevlar thread. The composite test articles were fabricated using Hercules, Inc. 3501-6 epoxy in a Resin Film Infusion (RFI) process which is described in references 13 and 14.

Two panels of each configuration were fully stitched and one was partially stitched. Stitching is a multi-step process. First, the skin region between stiffeners was stitched with rows approximately 6.3 mm (0.25 in.) apart while the region where flanges would be attached was initially not stitched. Second, blades were stitched such that stacks of material in the top half of the component were stitched and the bottom half were folded out so the bottom part would become the stiffener flange, as shown in figure 2. Third, in two panels of each configuration, the blades were positioned on the skin and the flanges stitched to the skin. In the third panel of each configuration, the stitching in step three was omitted. Finally the entire assembly was cured in the autoclave where the epoxy was added through a resin-film-infusion process. Specimens which were partially stitched did not have stitches holding the flange to the skin. These flanges were held to the skin by the resin through co-curing only, as in traditional graphite-epoxy structures. A photograph of a panel prior to testing is shown in figure 3.

To prevent end brooming during compressive loading, 25.4 mm on each end of each panel was encased in a potting compound. The ends of all panels were then ground flat and parallel prior to testing. Between 20 and 44 axial and lateral, back-to-back, strain gages were bonded to each panel.

Panels are identified by a configuration number, (1,2,3, or 4) herein. All configurations are defined in table 1. Letters indicate the degree of stitching and impact damage. Panels with flange-to-skin stitching are designated with an “s” and panels without flange-to-skin stitching are

designated with a “w.” Panels with no impact damage are called “control panels” and are identified with a “c.” Panels with impact damage are identified with an “i.” For example, the three panels with configuration 1 are identified as “1sc,” “1si” and “1wi.”

3. Impact Damage and Test Procedure

Two of the three specimens of each design configuration were impacted using a drop-weight impactor with a 25.4-mm-diameter tup prior to compressive loading. The impact energy level was selected based on criteria developed during the NASA-Boeing Advanced Composites Technology (ACT) Program [1,15] to represent “barely visible damage” to a wing skin. The design philosophy used was that impact energies greater than this level would be detected and repaired but damage that was “barely visible” might not be detected and therefore the wing would be required to carry DUL in the presence of this damage. Testing conducted during the early stages of the ACT program determined this energy level to be 135.5 J (100 ft-lb) [16]. This level of damage is also cited as one critical damage criteria in reference 17, which is a design guide for composite aircraft structures. For this reason, an impact energy of 135.5 J was imparted with each impact. However, even though 135.5 J was defined to be “barely visible,” damage resulting from such an impact can be quite visible when the skin is relatively thin. Panel skins were impacted on the unstiffened side opposite the base of a central stiffener. The location of the impact damage sites is shown in figures 1 and 2. Dent depths were measured with a depth gage and ultrasonic examination was used to determine the extent of the damage region. Measured dent depths are given in table 2. Four panels were impacted at two stiffener base locations. A photograph of the damage site of one panel is shown in figure 4. The dots around

the impact site in the photograph indicate the borders of the damage area. One panel with flange-to-skin stitching of each configuration was not damaged prior to loading. One panel with flange-to-skin stitching of each configuration was subjected to the drop weight impact damage prior to loading. The panel without flange-to-skin stitching of each configuration was also subjected to the drop weight impact damage prior to loading. All panels were loaded to failure at room temperature.

Specimens were loaded in axial compression in a 4450-kN-capacity (1 million-lb-capacity) test machine. Load rates varied among the different tests, but generally tests were planned to run for 15-30 minutes. Data were recorded at the rate of one frame each second as load was applied. Displacements were measured using two displacement transducers measuring end-shortening, three transducers measuring out-of-plane displacement at the midlength location midbay and one transducer measuring out-of-plane displacement in the central bay at the quarter of the length. Strain gages were used to monitor strains in the flanges, blades and skin regions. Typical strain gage and displacement measurement locations are shown in figure 3. The unstiffened side of each panel was painted white so that buckling mode shapes could be monitored by using moiré interferometry. Buckling loads, final failure loads, failure locations and failure modes were noted for each specimen. All panels were loaded until no additional loading could be sustained by the panel.

4. Analysis

A finite element analysis of each specimen configuration with no impact damage was conducted using the STAGS (SStructural Analysis of General Shells) structural analysis

code[18]. A discussion of nonlinear finite element analysis is presented in reference 19. The analysis accounts for geometric nonlinearities but not material nonlinearities. A buckling load was calculated based on a linear prebuckling stress state. Then a nonlinear analysis was conducted and buckling mode shapes were calculated based on the nonlinear stress state. Then an assumed initial imperfection in the shape of the buckling mode corresponding to the minimum buckling load was added. An imperfection mode with an amplitude of 0.025 mm (0.001 in.) was used to trigger nonlinear behavior for loads equal to and greater than the buckling load. Material properties are assumed to be: longitudinal stiffness, $E_x=6.37 \times 10^{10}$ Pa (9.25 Msi); transverse stiffness, $E_y= 3.22 \times 10^{10}$ Pa (4.67 Msi); shear stiffness, $G_{xy}= 1.56 \times 10^{10}$ Pa (2.27 Msi); major Poisson's ratio, $\nu=0.397$; allowable compressive strain= -0.0089 mm/mm; allowable tensile strain= 0.0121 mm/mm; density, $\rho= 1.58$ g/cm³ (0.057 lb/in³) [20].

All structural components were modeled using quadrilateral shell elements. The finite element model is shown in figure 5a and has 6,072 nodes and 5,916 elements, for a total of 36,432 degrees of freedom. All degrees of freedom were restrained on one end of the specimen and all degrees of freedom except axial motion were restrained on the other end. Axial motion was required to be the same for all nodes along the edge where the load was applied. The potting material was not modeled. The unloaded edges of the panel were not restrained.

An additional analysis was conducted of panel 1sc. This additional analysis used a finite element model of approximately 1/6 of the panel and the analytical technique described in reference 21 to determine the normal forces between the flange and skin. This local model is shown in figure 5b and is used to examine interlaminar forces between the flange and the skin. In this model the flange and skin are modeled as separate elements joined together by rigid links. As in reference 21, the link was required to be constant in length throughout loading and all

displacements and rotations of each flange node were required to be the same as the displacements and rotations of its linked skin node. Displacement boundary conditions were applied to the model edges, based on the analysis of the entire panel.

5. Results and Discussion

Analytical and experimental results are presented for four specimen configurations. A discussion of the control panels' behavior is first presented, followed by a discussion of the influence of impact damage and of flange-to-skin stitches. Buckling loads reported are the load at the onset of the initial buckling behavior and failure loads reported represent the maximum load the panel supported.

5.1 Control panels

One panel with each configuration was loaded to failure and each panel buckled prior to failure. Buckles were local to the skin bays between the stiffeners. Skin bays within a panel did not necessarily buckle at the same time. Of the panels with the thinnest blade, the panel with the thinnest skin (1sc) sustained a maximum load of 3.5 times the buckling load while the panel with the slightly thicker skin (2sc) sustained a maximum load of 1.7 times the buckling load. Of the panels with the thicker blade, the panel with the thinner skin (3sc) sustained a maximum load of approximately twice the buckling load and the panel with the thickest skin (4sc) failed shortly after buckling.

A photograph of panel 1sc subjected to a load of 734 kN (165,000 lb) is shown in figure 6a. The buckle pattern is easily determined by the use of moiré interferometry to highlight out-

of-plane displacements. Buckles shown in figure 6a form in all skin bays at this load level. The analytical prediction of the out of-plane deformations of this panel at a load of 757 kN (170,000 lb) is shown in figure 6b and is consistent with the experimental results. Experimental and analytical results of out-of-plane deformations for this panel at a load of approximately 2,225 kN (500,000 lb) are shown in figures 6c and 6d, respectively. These results show fully-formed buckle patterns in all skin bays. Five half-waves can be seen in the moiré patterns in the two outer skin bays and six half-waves in the central bay. Five half-waves are predicted in each bay. The panel failed at a load of 2,510 kN (564,000 lb) and a photograph of this failed panel is shown in figure 7. Deformation patterns for the other control panels, 2sc, 3sc, and 4sc, are shown in figures 8, 9, and 10, respectively. The panel with the thickest skin and the thickest blade (4sc) began to buckle in the central bay prior to failure, but buckles in the outer bays did not fully form prior to failure.

Panels 1sc, 3sc and 4sc failed at the midlength location and also exhibited local skin-flange separation, including broken stitches. Panel 2sc did not fail midlength, but rather approximately at a quarter of the length from the bottom, but also with local skin-flange separation. All control panels failed across the full width of the panel.

Using the technique described in reference 21 and the local model of panel 1sc, the shear and normal forces between the flange and skin were calculated and found to not reach the combined allowables described in the reference. Therefore, the forces between the flange and skin alone are not large enough to cause the skin and flange to separate in the stitched panels. In panel 1sc the flange stays relatively flat while the unsupported skin between the flanges buckles. The in-plane forces trigger the failure, but the stitches contain the damage and prevent propagation. Audible failures were recorded at loads significantly less than the failure loads for

all control panels. Buckling and failure loads for all control panels are shown in figure 11 where the open symbols represent the predicted buckling loads, the filled symbols represent the experimental buckling loads. Experimental and predicted buckling loads are in good agreement. Failure loads of the control panels are represented by solid bars. Control panels supported loads of 1.1 to 3.5 times the buckling load.

5.2 Impact-damaged panels

Two panels of each configuration were subjected to impact damage prior to compressive loading. All impact-damaged panels failed at loads less than their comparable control panels, as shown in figure 11 where the cross-hatched bars represent failure loads of the impact-damaged panels. Buckling loads were not as severely effected by impact damage compared to the failure loads. As illustrated in the figure, the failure loads of the control panels are 10-20 percent greater than failure loads of the panels with skin-to-flange stitching and impact damage. The failure loads of the control panels are 20-40 percent greater than the failure loads of the impact-damaged panels without skin-to-flange stitching. Photographs of comparable stitched and unstitched impact-damaged panels with configuration 1 are provided in figures 12 and 13, respectively, to demonstrate the difference in failure modes. There is little difference in the appearance of the failed stitched control panel shown in figure 7 and the failed stitched impacted panel shown in figure 12. Neither stitched panel demonstrates significant skin-stiffener separation. However, without stitching, the flange can separate from the skin over lengths greater than 140 mm, as shown in figure 13. Stitching suppresses this delamination and limits the damage region. While stitching does not bring the impact-damaged panels failure loads up

the level of the control panels, it can improve the load carrying capability of damaged panels. Similar damage is seen in the failed panels of other configurations.

If impact damage tolerance is the critical criterion for design of compression panels which are expected to operate into the postbuckling region, stitching can increase the design loads for minimum gage panels. A comparison of weight and failure loads for the four configurations of panels is shown in figure 14. Panel weight ranged from 70N (15.8 lb) for configuration 1 to 116 N (26.1 lb) for configuration 4. Failure loads for the twelve tested panels are shown in figure 14a where open bars represent control panels and cross-hatched bars represent impact-damaged panels. Buckling and failure loads are normalized by the buckling load of the control panels and are shown in figure 14b where open symbols represent buckling loads and filled symbols represent failure loads. Based on a percentage of load, the largest benefit of stitching is for the lightest weight panels, where the impact-damaged panel with the stitched flange supported 30% more load than the impact-damaged panel without stitching through the flange. Less than a 5% increase in failure load due to stitching can be seen in the other three configurations.

6. Concluding Remarks

The structures examined in this study are designed to be representative of the wing cover panel of a commercial transport aircraft. Results indicate that the presence of through-the-thickness stitches between the stiffener flange and the skin can suppress the separation of the flange from the skin of graphite-epoxy compression-loaded panels loaded to loads significantly greater than the buckling load. A comparison of stitched and unstitched panels with impact

damage indicates that while stitching does not consistently increase the panel buckling load, stitching can increase the failure loads by up to 30%.

References

- [1] Karal M. AST Composite Wing Program - Executive Summary. NASA CR 2001-210650. August 2001.
- [2] Jegley D, Bush H, Lovejoy A. Structural Response and Failure of a Full-Scale Stitched Graphite-Epoxy Wing. *Journal of Aircraft* Nov. Dec. 2003. Vol. 40: p.1192-1199.
- [3] Starnes JH Jr., Knight NF Jr., Rouse M. Postbuckling Behavior of Selected Flat Stiffened Graphite-Epoxy Panels Loaded in Compression. *AIAA Journal* 1985 Vol 23 no. 8: p. 1236-1246.
- [4] Hyer MW, Loup DC, Starnes, JH Jr. Stiffener/Skin Interactions in Pressure-Loaded Composite Panels. *AIAA Journal* 1990 Vol 28 no. 3: p. 532-537.
- [5] Bonanni DL, Johnson ER, Starnes, JH Jr. Local Crippling of Thin-Walled Graphite-Epoxy Stiffeners, *AIAA Journal* Nov 1991. Vol 29, no 11: p. 1951-1959.
- [6] Agarwal BL. Postbuckling Behavior of Composite Shear Webs, *AIAA Journal* July 1981 Vol 19 No 7: p. 933-939.
- [7] Wang C, Pian THH, Dugunji J, Lagace, PA. Analytical and Experimental Studies on the Buckling of Laminated Thin-Walled Structures. Presented at the 28th AIAA/ASME/ASCE/AHS/ASC Structures, Structural Dynamic and Materials Conference, Monterey CA, 1987. AIAA paper no. 87-727.

- [8] Rehfield LW, Reddy AD. Observations on Compressive Local Buckling, Postbuckling Crippling of Graphite/Epoxy Airframe Structure. Presented at the 27th AIAA/ASME/ASCE/AHS/ASC Structures, Structural Dynamic and Materials Conference, Williamsburg VA, 1986. AIAA paper no 86-923-727.
- [9] Glaessgen EH, Raju IS, Poe, CC Jr. Delamination and Stitched Failure in Stitched Composite Joints. Presented at the 40th AIAA/ASME/ASCE/AHS/ASC Structures, Structural Dynamic and Materials Conference, St. Louis MO, 1999. AIAA paper no. 99-1247.
- [10] Raju IS, Glaessgen EH. Effect of Stitching on Debonding in Composite Structural Elements. Presented at the International Conference on Computational Engineering and Sciences, Puerto Vallarta, Mexico, Aug 2001.
- [11] Starnes JH Jr., Rhodes MD, Williams JG. Effect of Impact Damage and Holes on the Compressive Strength of a Graphite/Epoxy Laminate Nondestructive Evaluation and Flaw Criticality for Composite Materials. ASTM SP 696 edited by R B Pipes, American Society of Testing and Materials, Philadelphia, PA, 1979: p. 145-171.
- [12] Starnes JH Jr. Buckling and Postbuckling Research on Flat and Curved Composite Panels, Selected NASA Research in Composite Materials and Structures, NASA CP-2142, 1980: p.313-327.
- [13] Markus A, Thrash P, Grossheim B. Manufacturing Development and Requirements for Stitched/RTM Wing Structure. NASA CP 3229. 1993: p. 503-523.
- [14] Rohwer K, Ghumman A, Markus A. Stitched/Resin Film Infusion (S/RFI) Manufacturing Technology Development. Proceedings of the 11th DOD/NASA/FAA Conference on

- Fibrous Composites in Structural Design. Report Number WL-TR-97-3009: p. XIII-93-116.
- [15] Davis, JG Jr. Overview of the ACT Program. Proceedings of the Ninth DoD/NASA/FAA Conference on Fibrous Composites in Structural Design, 1991: p. 577-599.
- [16] Madan, RC, Sutton, JO, Design, Testing and Damage Tolerance Study of Bonded Stiffened Composite Wing Cover Panels. Presented at the 29th AIAA/ASME/ASCE/AHS/ASC Structures, Structural Dynamic and Materials Conference, Williamsburg VA, 1988. AIAA paper no. 88-2291.
- [17] Niu MCY. Composite Airframe Structures, Practical Design Information and Data. Conmilit Press Ltd, Hong Kong, 1992.
- [18] Rankin CC, Brogan FA, Loden WA, Cabiness HD. STAGS User Manual, Version 3.0. Lockheed Martin Missiles and Space Company, Incorporated. March 1999.
- [19] Knight NF. Finite Element Techniques of Nonlinear Postbuckling and Collapse of Elastic Structures. In: Leondes CT, editor. Structural Dynamic Systems Computational Techniques and Optimization, Finite Element Analysis Techniques. Australia: Gordon and Breach Science, 1998: p. 1-95.
- [20] Hinrichs, S. General Methods for Determining Stitched Composite Material Stiffnesses and Allowable Strengths, Volume I, McDonnell Douglas Rept MDC94K9113, Long Beach, CA, March 1995.
- [21] Jegley DC. Behavior of Compression-Loaded Composite Panels with Stringer Terminations and Impact Damage. Journal of Aircraft. Nov.-Dec. 1999: p.1048-1054.

Table 1. Geometry and buckling behavior of control panels.

Configuration designation	Skin thickness (mm)	Blade thickness (mm)	Blade height (mm)	Predicted buckling load (kN)	Measured buckling load (kN)
1sc	330	112.	65.4	810	712
2sc	450	112.	65.4	1,566	1,513
3sc	410	140.	82.3	1,900	2,002
4sc	620	140.	82.3	4,347	4,005

Table 2. Impact damage descriptions^a

Panel identification	Dent depth mm	
1sc	N.A.	
1si ^b	0.6	0.5
1wi ^b	1.8	1.7
2sc	N.A.	
2si ^b	0.6	0.5
2wi ^b	0.9	0.0
3sc	N.A.	
3si	0.4	
3wi	0.6	
4sc	N.A.	
4si	0.4	
4wi	0.5	

^a All impacts were 135.5 J of impact energy to the panel skin

^b Two impacts on the same panel

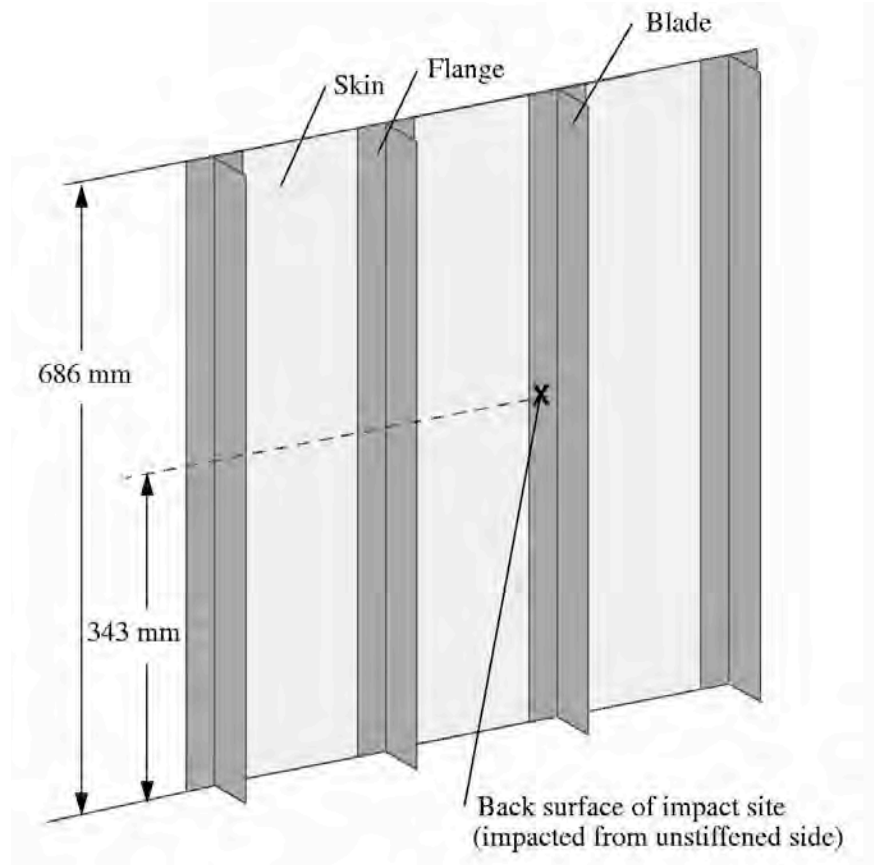


Figure 1. Sketch of panel.

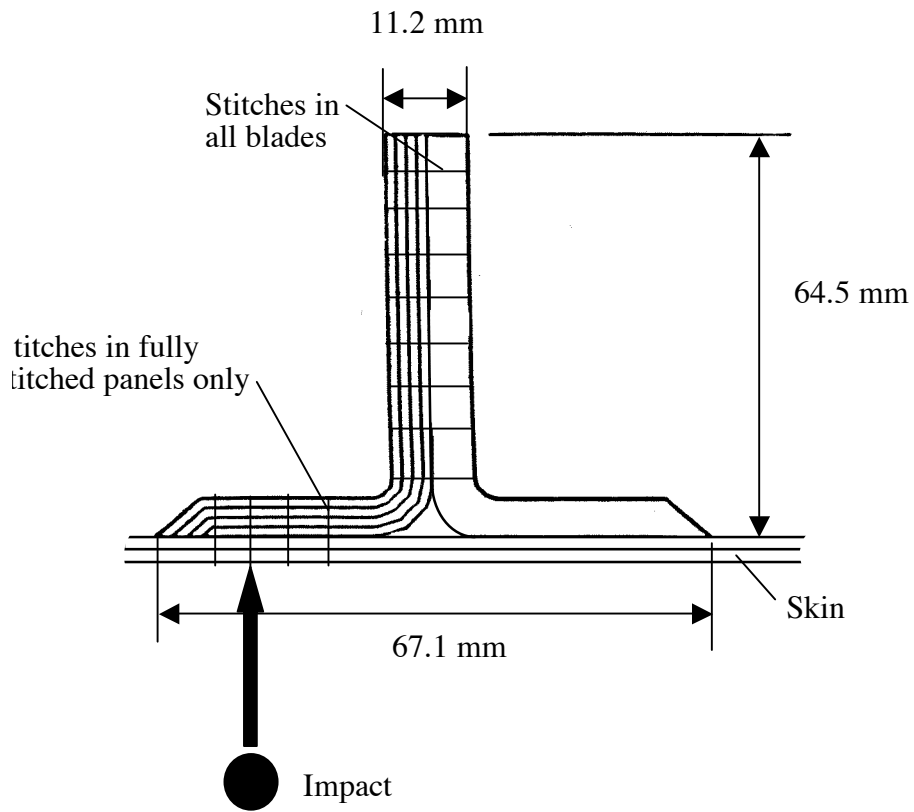
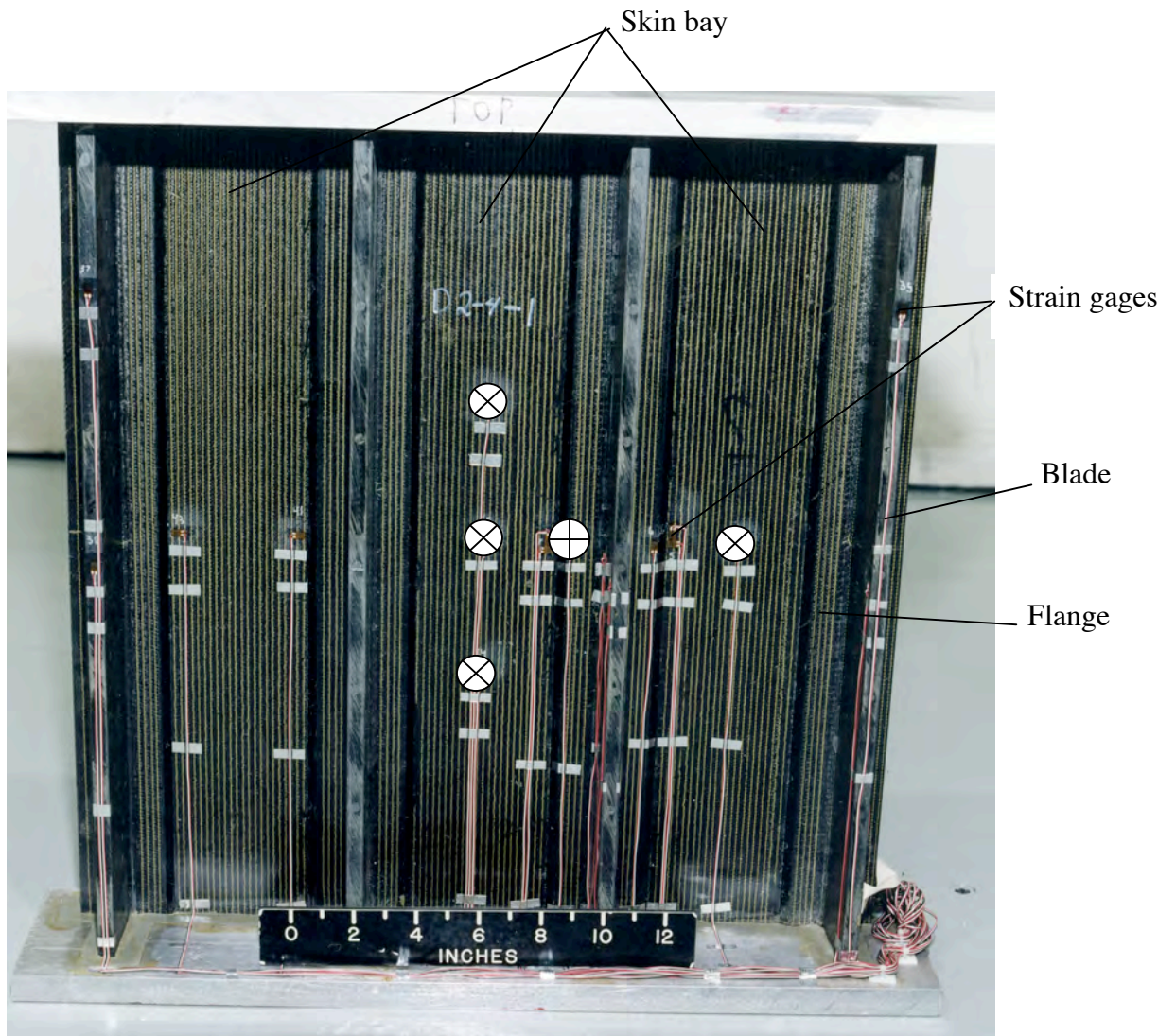


Figure 2. Sketch of blade and flange.



⊗ Out-of-plane displacement measurement location

⊕ Impact site location on untiffened side

Figure 3. Stiffened panel prior to testing.

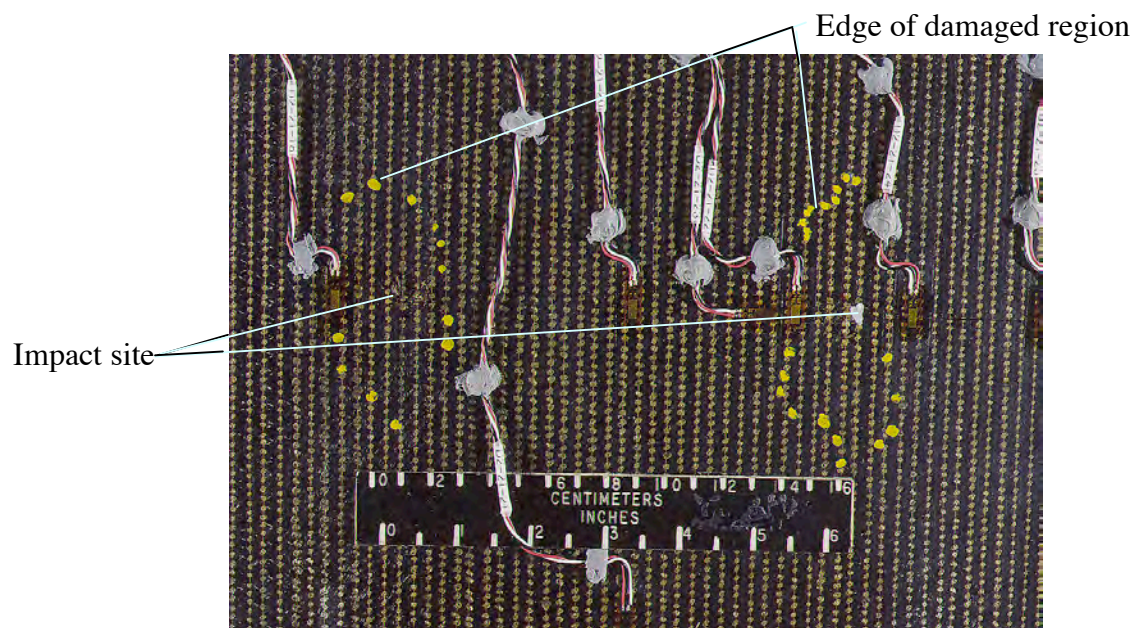


Figure 4. Impact-damage sites.

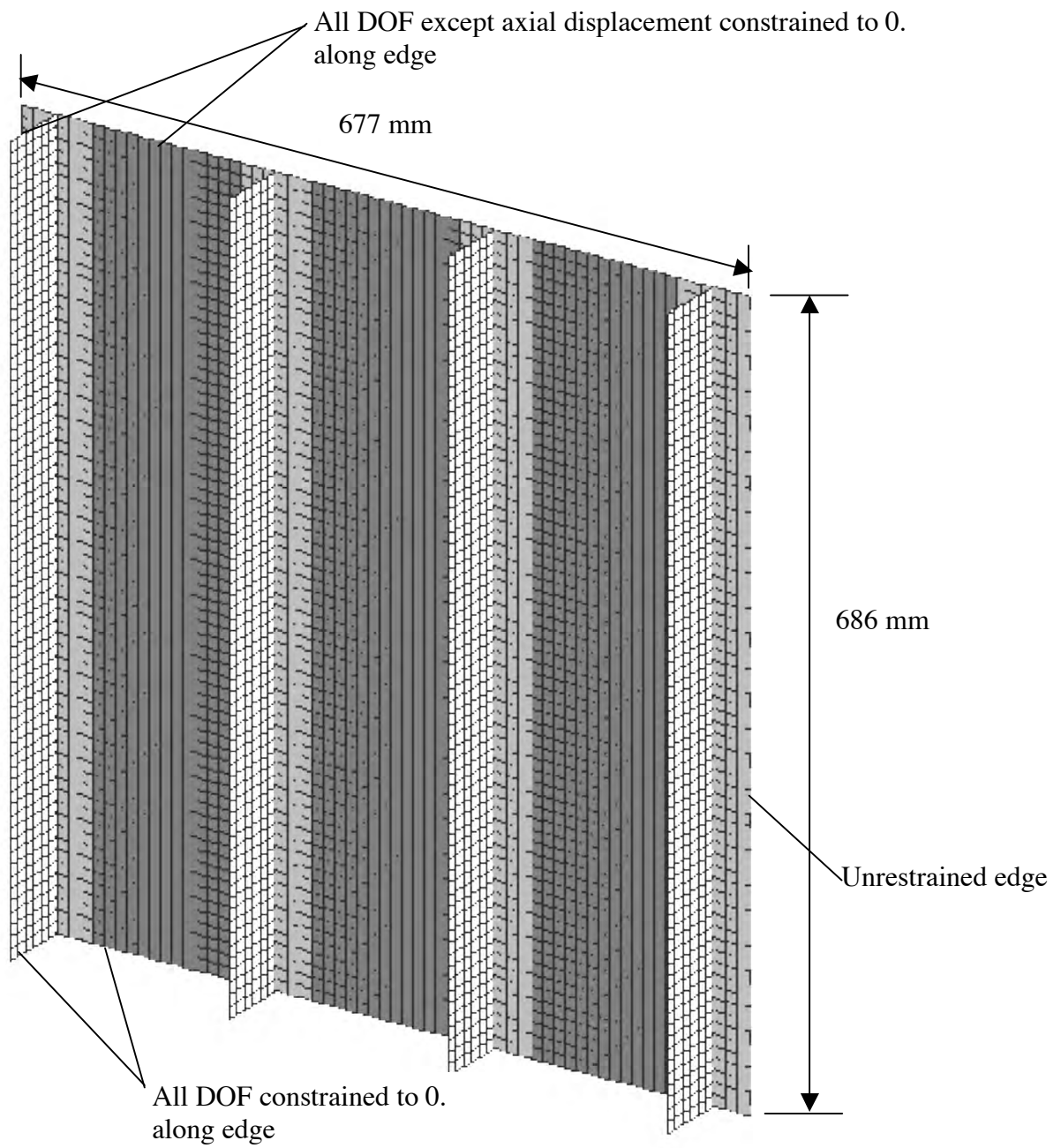


Figure 5a. Finite element model of panel.

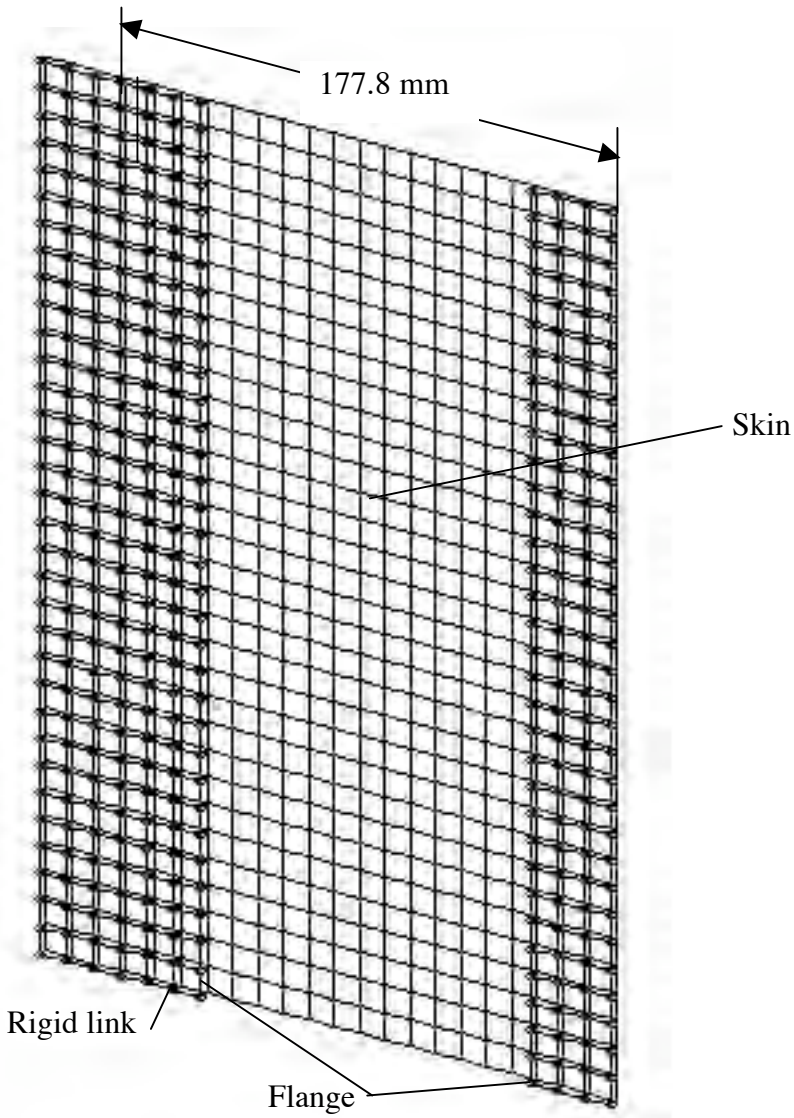


Figure 5b. Local finite element model.

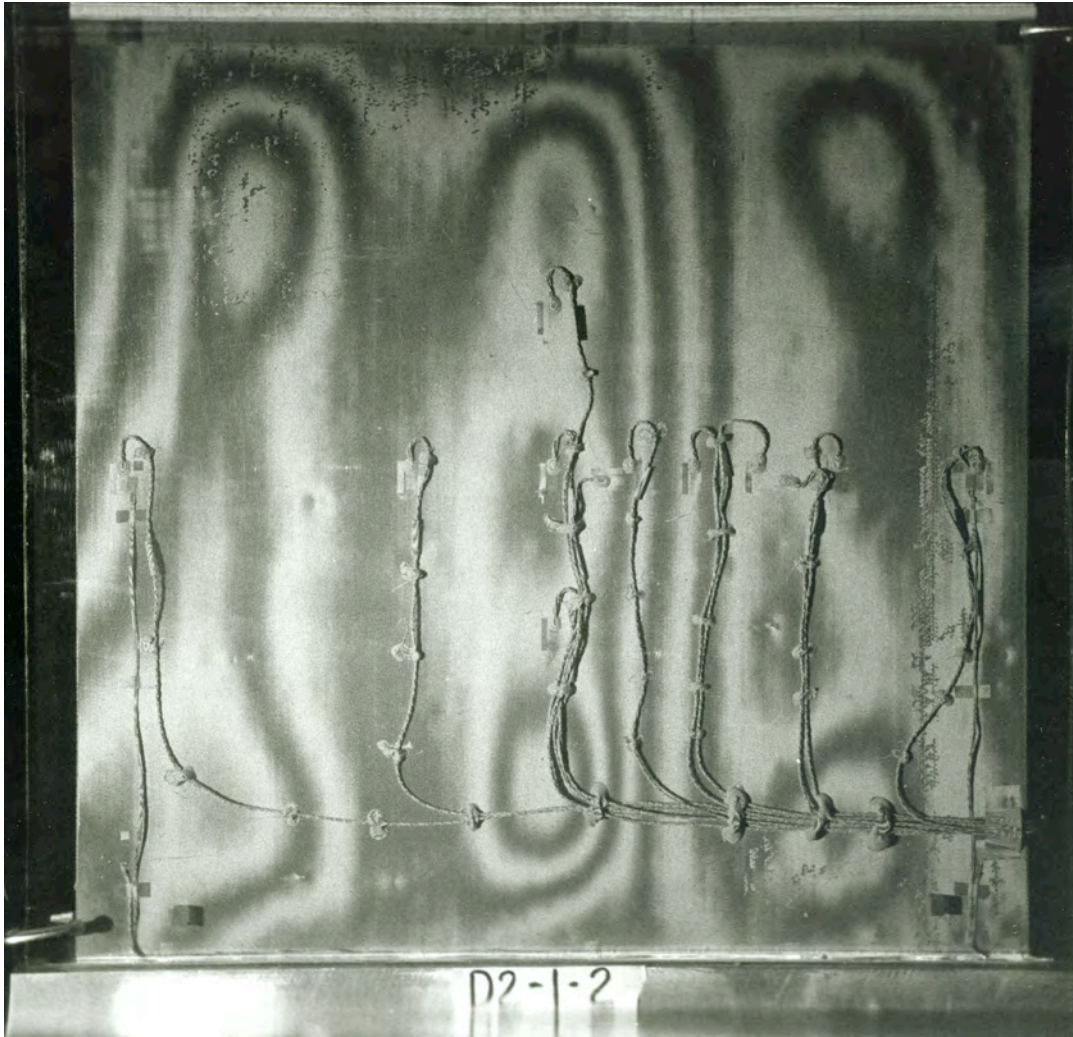


Figure 6a. Experimentally determined out-of-plane deformation pattern of panel 1sc with a load of 734 kN.

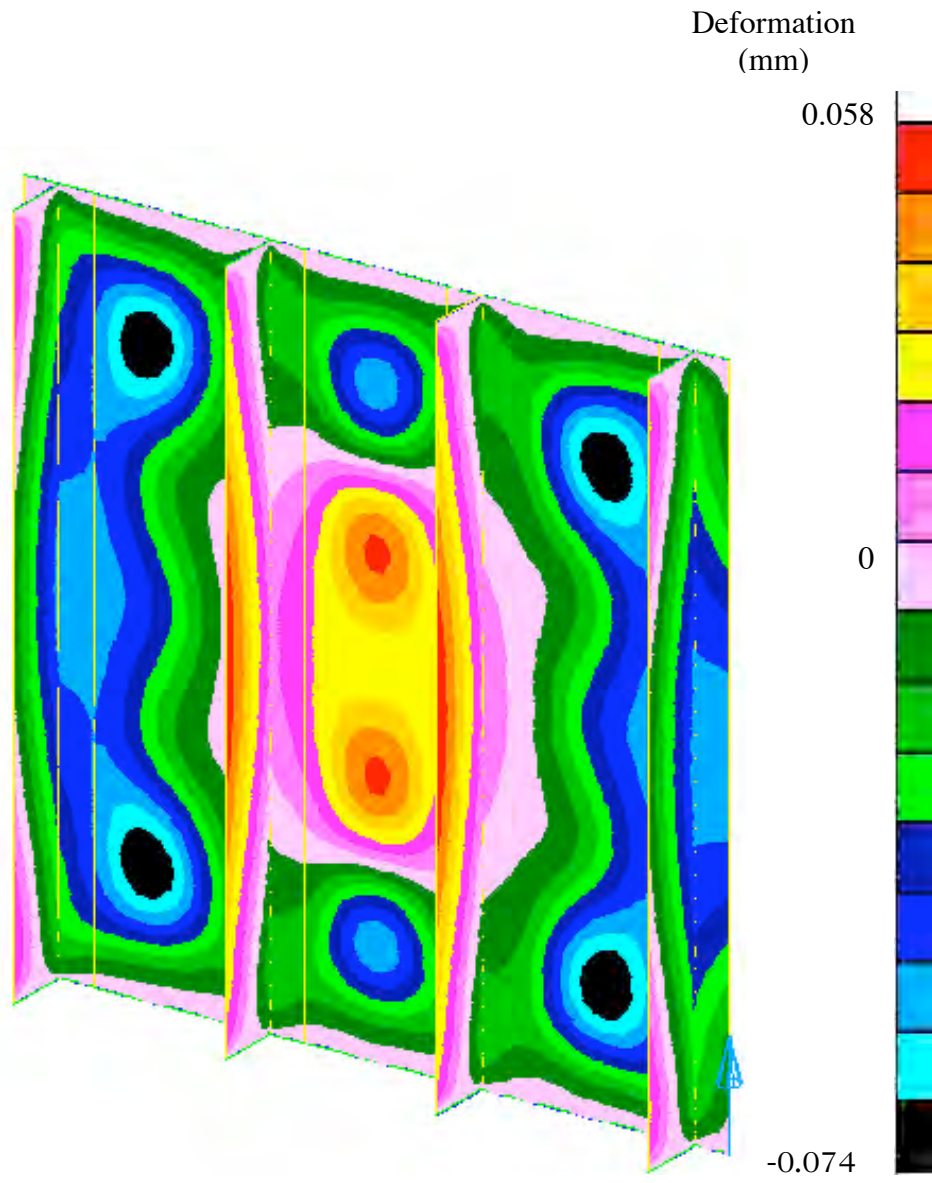


Figure 6b. Predicted out-of-plane deformation of panel 1sc with a load of 756.5 kN.

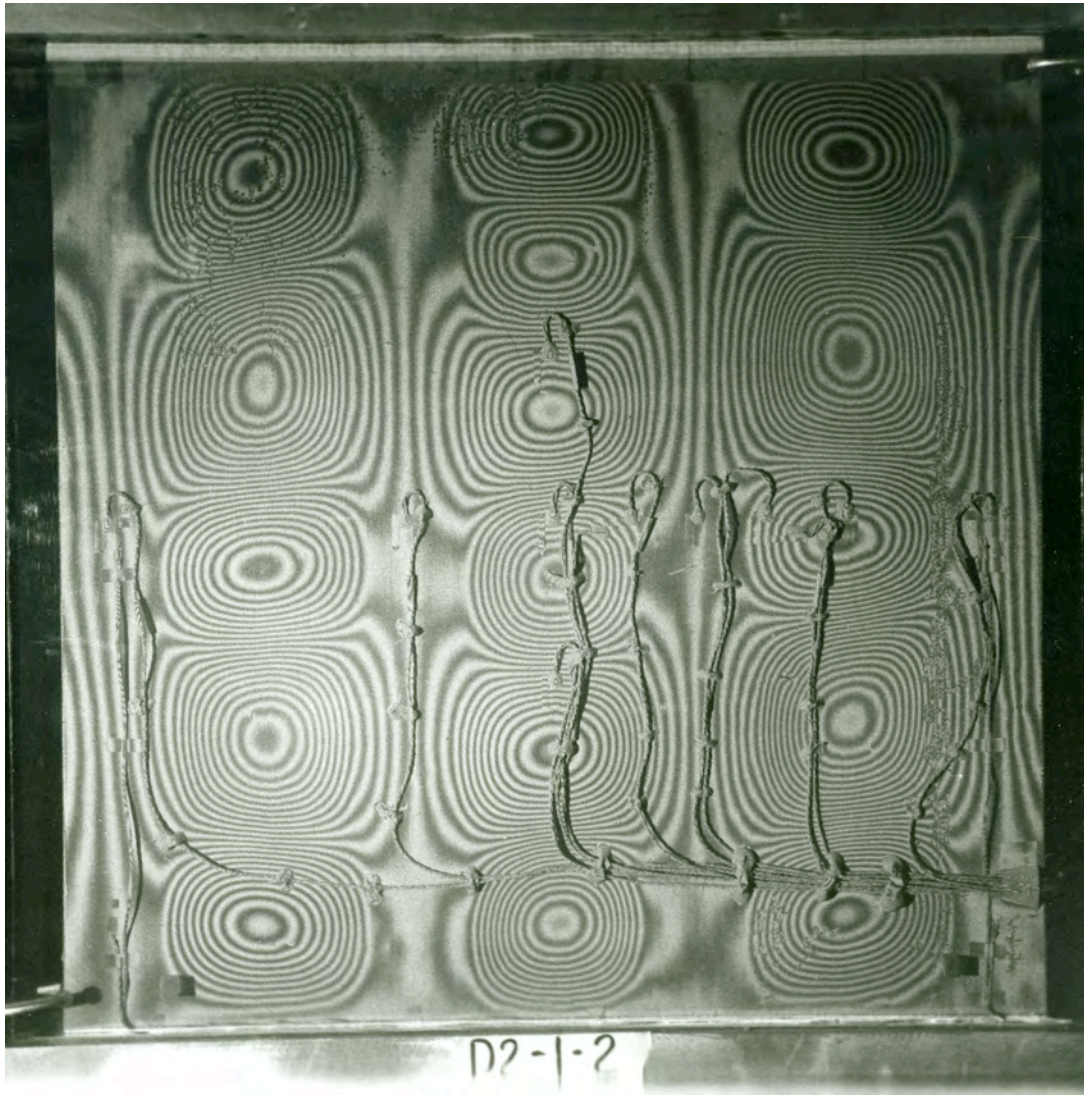


Figure 6c. Experimentally determined out-of-plane deformation pattern of panel 1sc with a load of 2,247 kN.

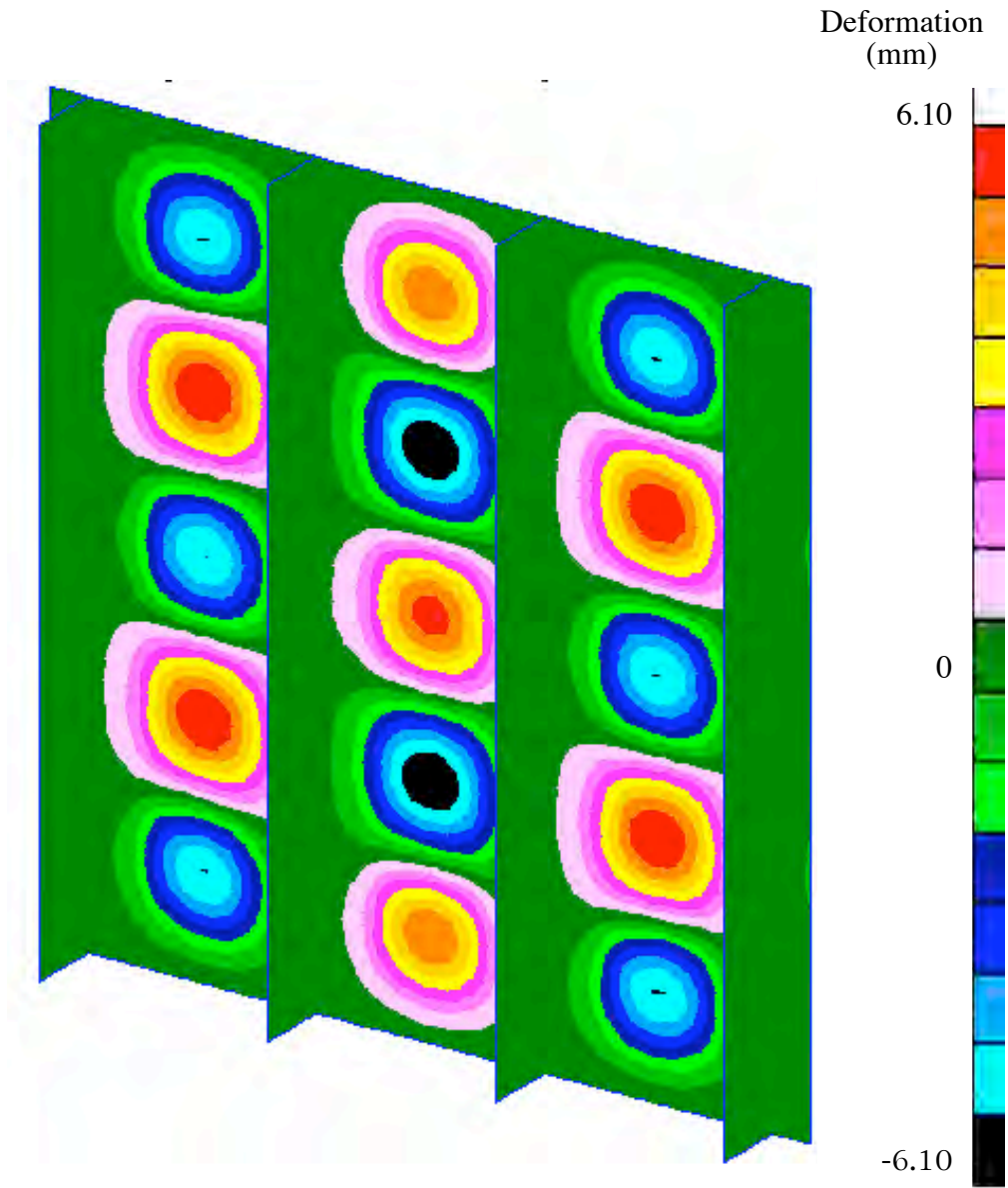
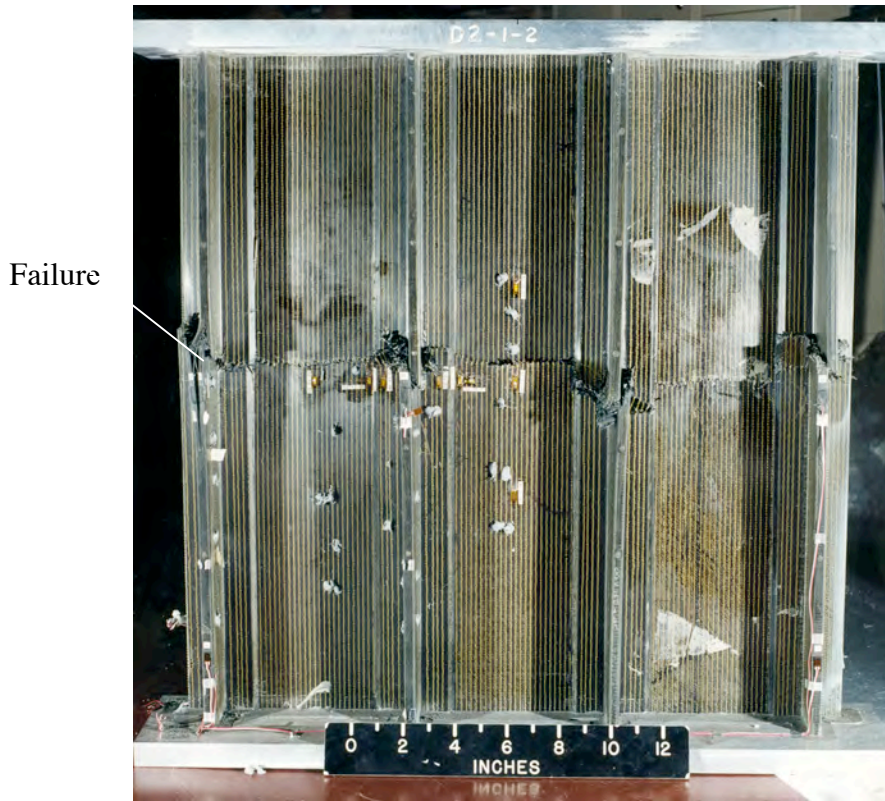


Figure 6d. Predicted out-of-plane deformation of panel 1sc with a load of 2,225 kN.



a) Failure across panel width.



b) Failed blade and flange.

Figure 7. Failure of panel 1sc.

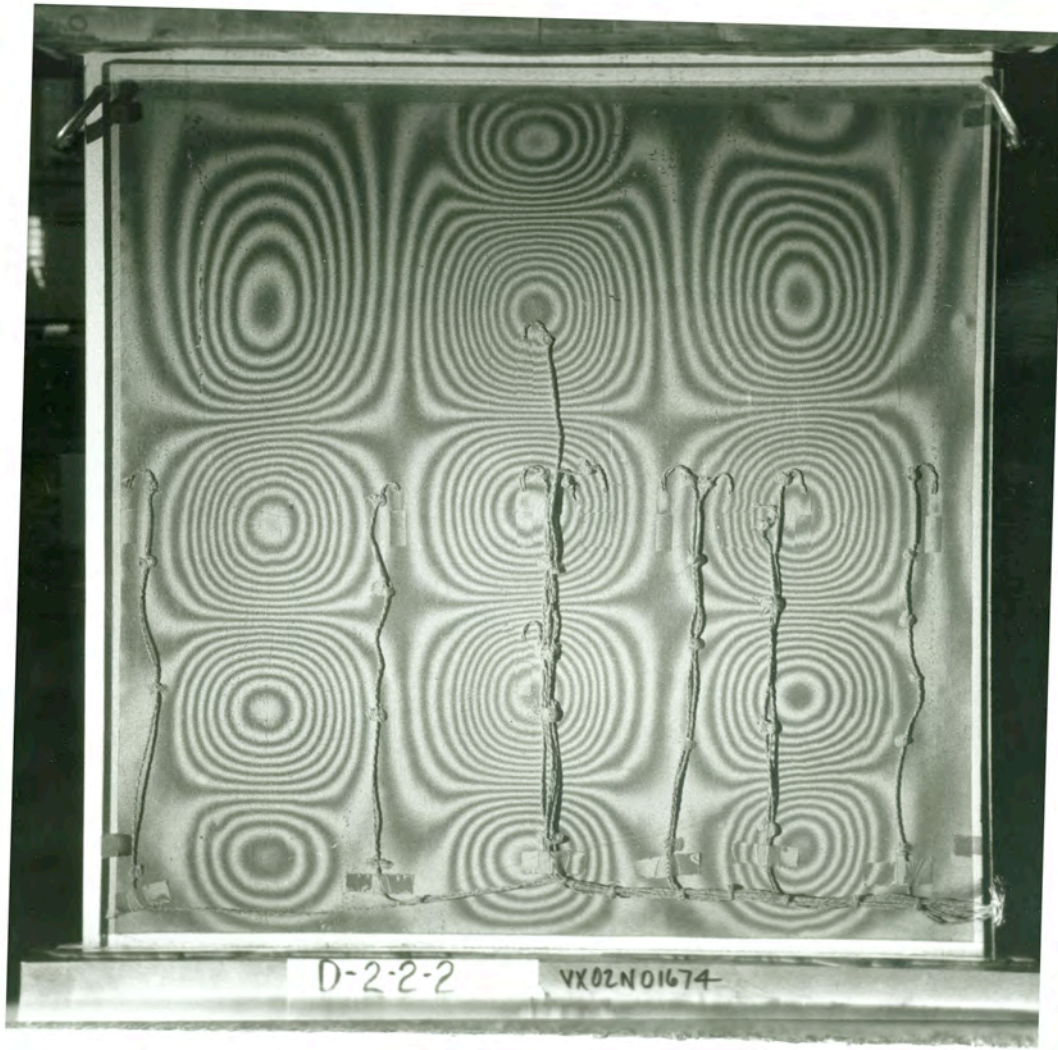


Figure 8. Experimentally determined out-of-plane deformation pattern of panel 2sc with a load of 512 kN.

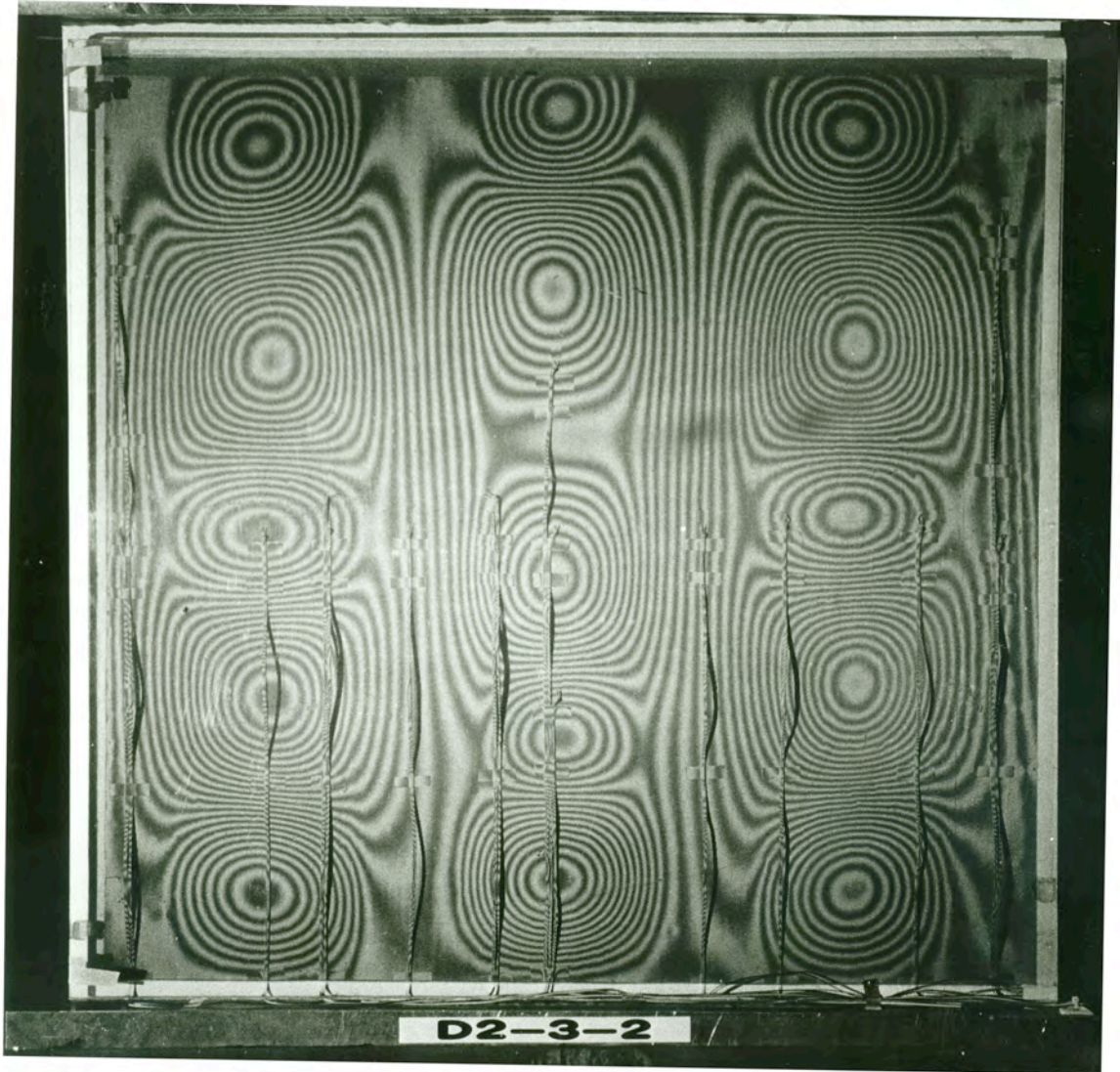


Figure 9. Experimentally determined out-of-plane deformation pattern of panel 3sc with a load of 3,690kN.

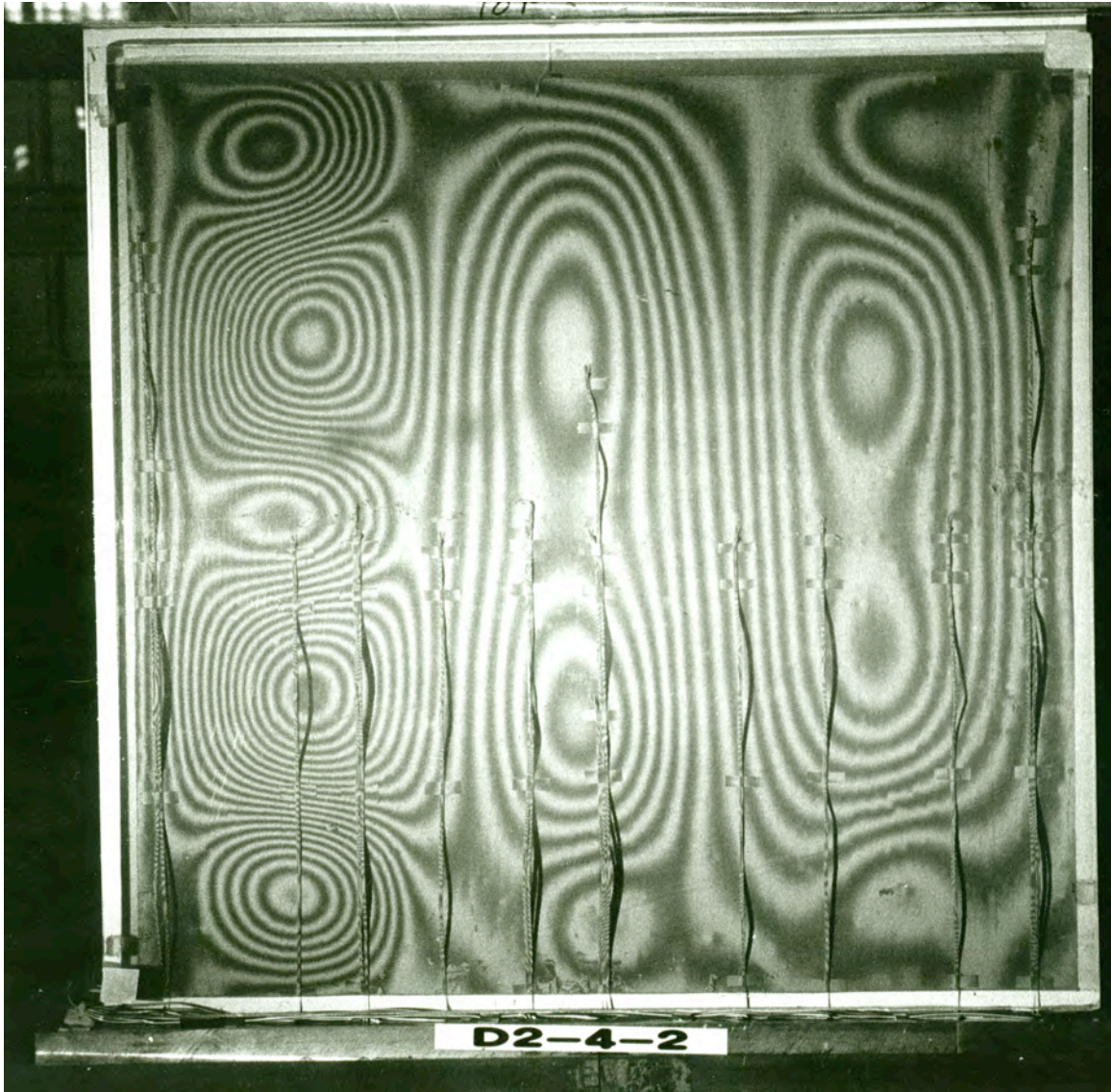


Figure 10. Experimentally determined out-of-plane deformation pattern of panel 4sc a load of 4,290 kN.

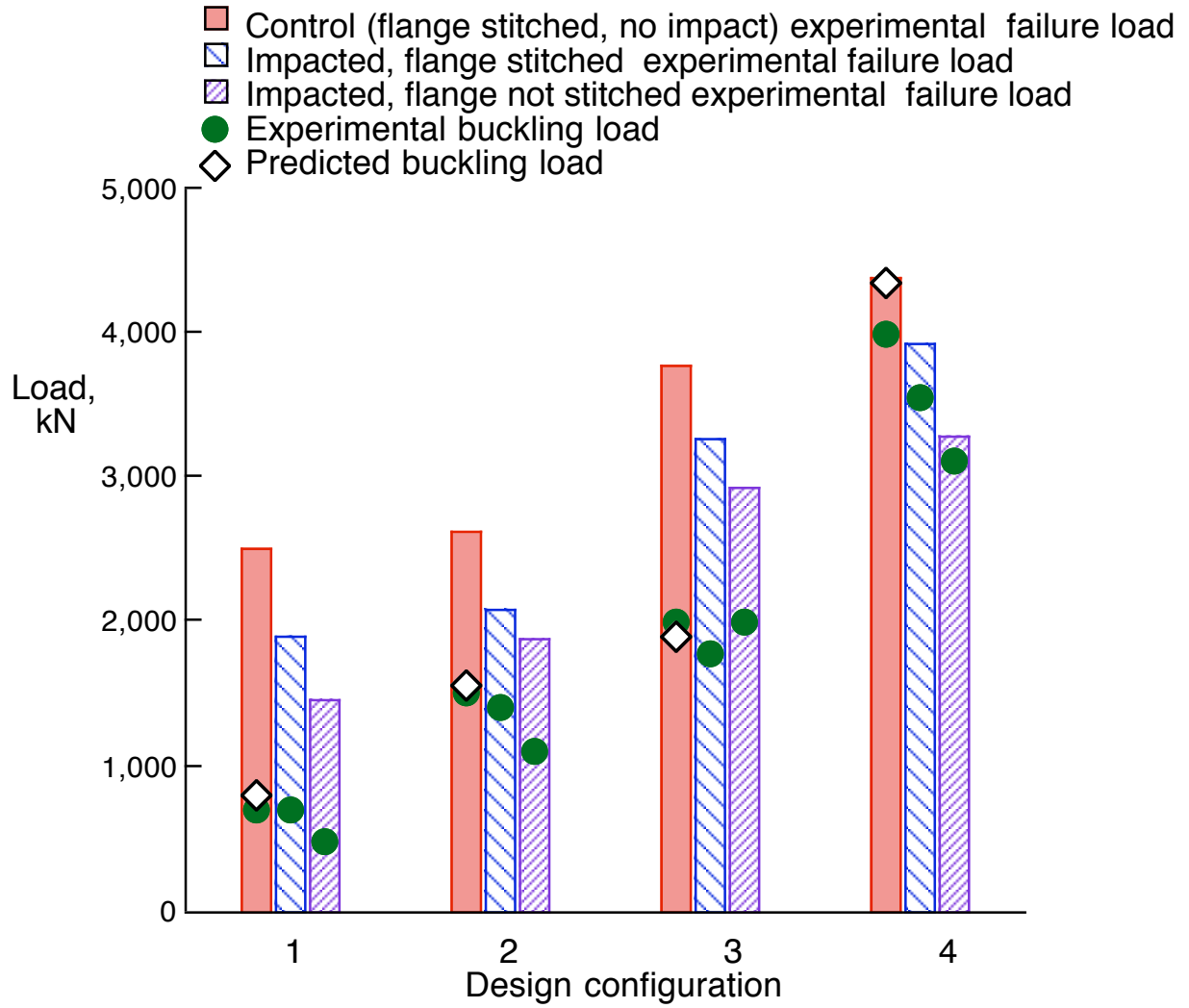
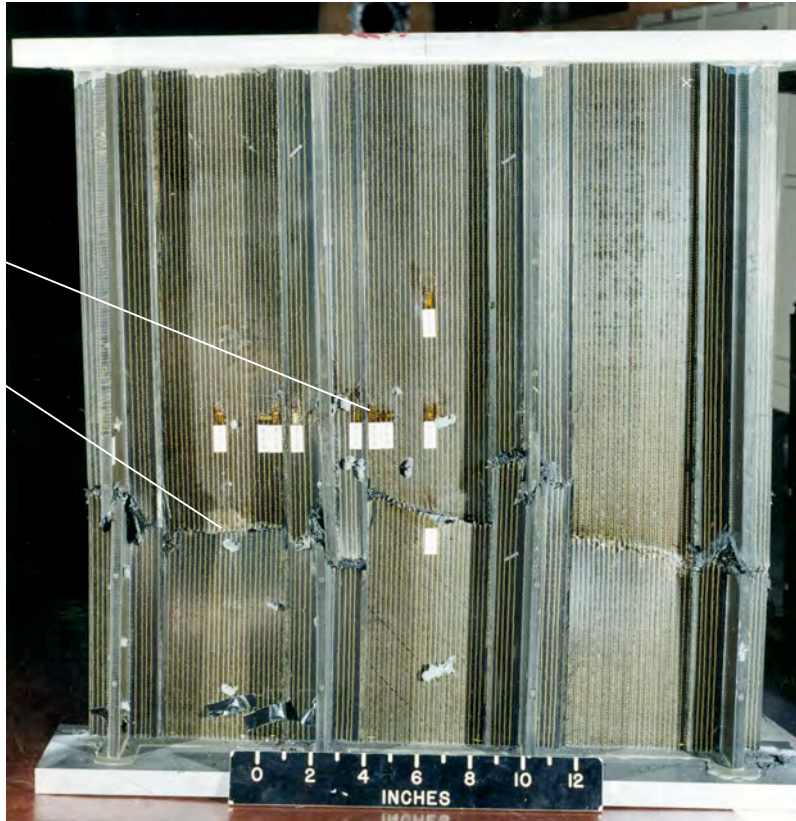


Figure 11. Buckling and failure load for all configurations.

Back surface of impact site

Failure



a) Failure across width.

Failure



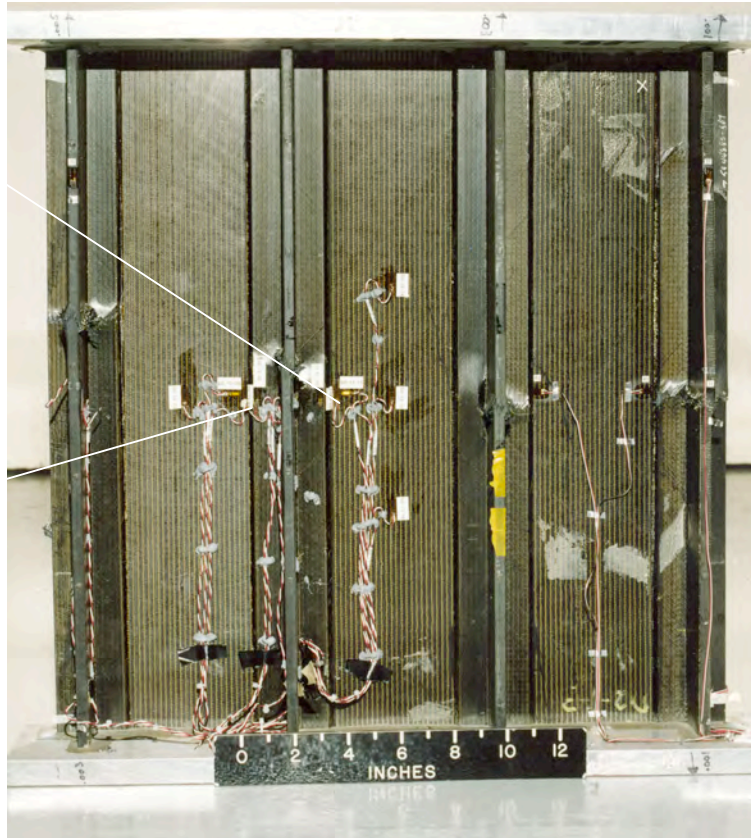
Blade

Flange

b) Failed blade and flange.
Figure 12. Failure of panel 1si.

Back surface of impact site

Failure



a) Failure across width.

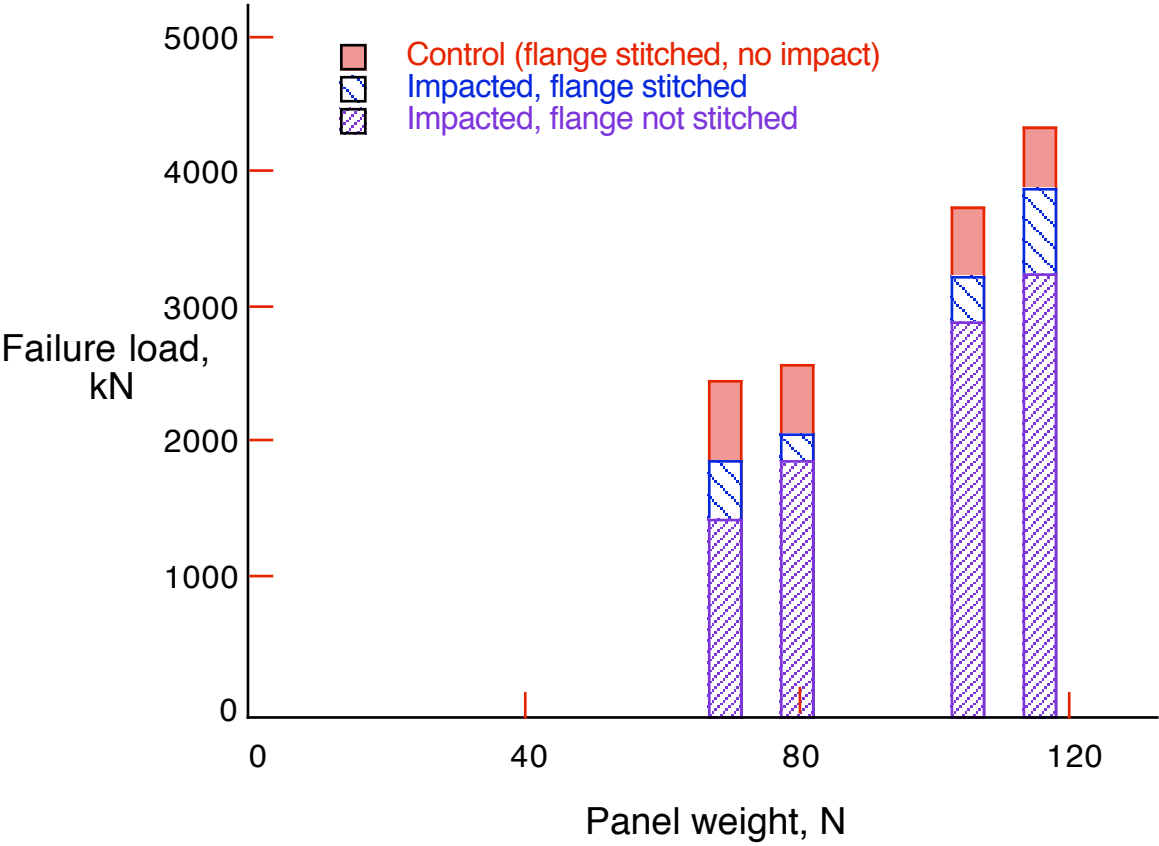
Delamination

Back surface of impact site

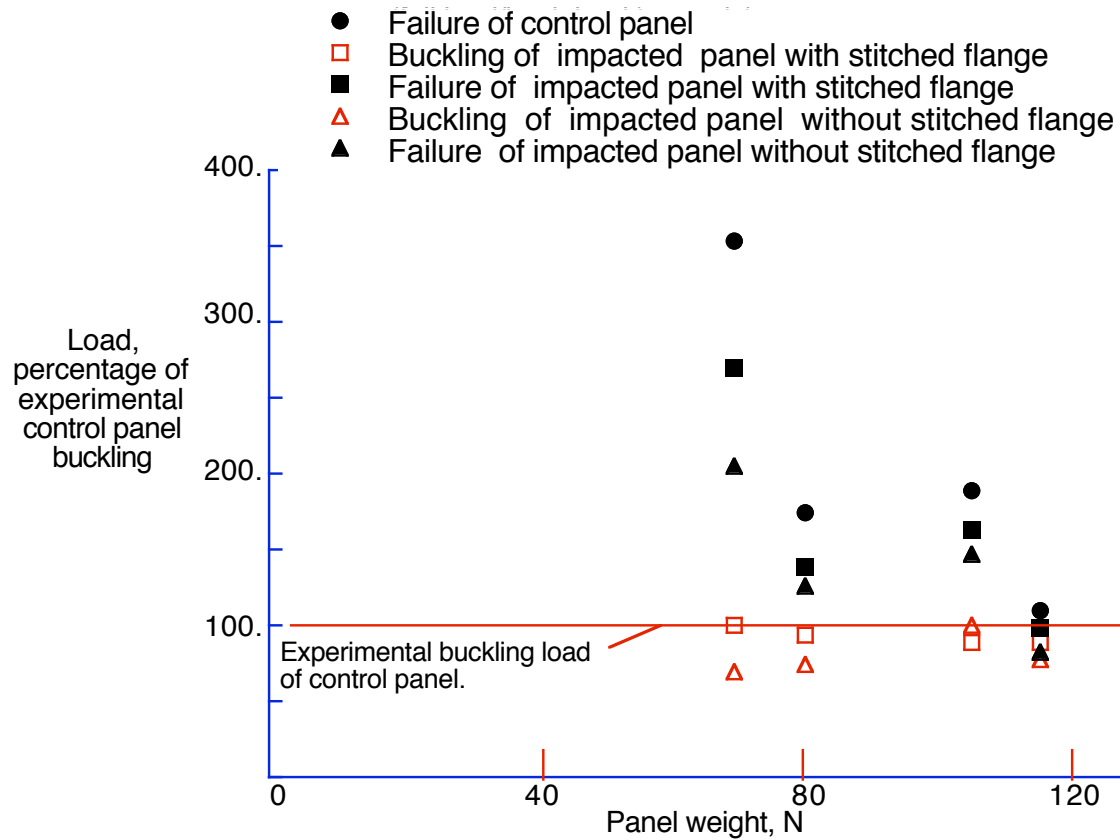
Broken blade



b) Failed blade and flange.
Figure 13. Failure of panel 1wi.



a) Panel failure load-weight relationship.



b) Experimental failure and buckling loads as a percentage of control panel buckling load

Figure 14. Panel failure loads.